Automatic Extraction of Pathological Area in 2D MR Brain Scan

P. Dvorak[1, 2], K. Bartusek[2], and E. Gescheidtova[3]

[1]Department of Telecommunications, Faculty of Electrical Engineering and Communication
Brno University of Technology, Technicka 12, Brno 612 00, Czech Republic
[2]Institute of Scientific Instruments of the ASCR
v.v.i., Kralovopolska 147, Brno 612 64, Czech Republic
[3]Department of Theoretical and Experimental Electrical Engineering
Faculty of Electrical Engineering and Communication, Brno University of Technology
Technicka 12, Brno 612 00, Czech Republic

Abstract— The aim of this work is to propose the fully automated pathological area extraction. The proposed method is based on multi-resolution symmetry analysis and automatic thresholding. The multi-contrast MRI (T2 and FLAIR images) is used. Since the method is based on symmetry, it works for both axial and coronal planes. In these both planes of healthy brain, the approximate left-right symmetry exists and it is used as the prior knowledge for searching the approximate pathology location. The algorithm was tested on 357 axial and 443 coronal real images from publicly available BRATS databases containing 3D brain volumes afflicted by a brain tumor. The results were evaluated by Dice Coefficient (axial: 0.85 ± 0.11, coronal 0.82 ± 0.18) and by Accuracy (axial: 0.96 ± 0.05, coronal 0.94 ± 0.09).

1. INTRODUCTION

Nowadays, the issue of automatic analysis of brain tumors is of great interest. It is the first step in surgical and therapy planning. And the very first step of the automatic analysis of brain tumor is its detection and subsequent segmentation. The detection of brain tumors is generally a more complex task than the detection of any other image object. Pattern recognition usually relies on the shape of the required objects. Since the tumor shape varies in each case, other properties have to be used. Several different and interesting methods have been developed in recent years. The existing algorithms can be classified into semi- and fully-automatic methods.

The semi-automatic [1, 2] require some user interaction, e.g., to select the starting point lying inside the tumor or to select several points of foreground and several points of background. The automatic [3, 4] methods do not require any interaction and are usually based on prior knowledge of the human brain structure, either tissue atlas or left-right symmetry, or their combination.

2. METHODOLOGY

In this work, for the better performance, the usage of multi-contrast MR is suitable. FLAIR and T2-weighted images are used. In both images, the pathological areas are well visible. Compared to the T1CE images, which is the most common contrast used in tumor segmentation, these contrasts do not require the contrast agent fluid.

The reason for multi-contrast MRI is much better differentiation of particular tissues than in case of using only one contrast image. E.g., the edema reaches similar intensities as CSF (Cerebro-Spinal Fluid) in T2-weighted images, while in FLAIR images, the intensities are absolutely different. On the other hand, the differentiation between necrosis and white matter is much better in T2-weighted images. That method is based on multi resolution symmetry analysis.

The input of the whole process are stand-alone registered 2D T2 and FLAIR magnetic resonance images. No neighbor slices are considered. The reason for these contrast images is the good visibility of this kind of pathology in them.

2.1. Preprocessing

The preprocessing consists of brain extraction, image registration and the symmetry axis detection. None of these parts is the aim of this work, but for this purpose, the existing algorithms described in [5–7] can be used for brain extraction, image registration and symmetry axis detection, respectively. Addition of such methods as a preprocessing step is the aim of future work.

2.2. Symmetry Analysis

The most important part of the presence detection process is the detection of symmetry anomalies, which are usually caused by a brain tumor, whose detection is the main purpose of this article. The first step of this process is dividing the input image into two approximately symmetric halves. Assuming that the head is not rotated and the skull is approximately symmetric, the symmetry axis is parallel to the vertical axis and divides the image of the detected brain into two parts of the same size. Since the method is not pixel-based, the precision of the determined symmetry axis does not have significant influence.

A squared block, with the side length computed as one quarter of the cropped image side length, is created. This size and sizes computed in the following computation are suitable for the detection of both small and large tumors. The algorithm goes through both halves symmetrically by this block. The step size is smaller than the block size to ensure the overlapping of particular areas. These areas are compared with their opposite symmetric part. In this case, the step size of one eighth of the block size was set.

A omparison is done by the Bhattacharya Coefficient [8]. Normalized histograms with the same range are computed from both parts and the Bhattacharya Coefficient (BC) is computed from these histograms as follows [8]:

$$\mathrm{BC} = \sum_{i=1}^{N} \sqrt{l\,(i) \cdot r\,(i)}, \tag{1}$$

where N denotes the number of bins in the histogram, l and r denote histograms of blocks in left and right half, respectively. The range of values of BC is $\langle 0; 1\rangle$, where the smaller the value, the bigger the difference between histograms. For the next computation, the asymmetry is computed as:

$$A = 1 - B. \tag{2}$$

This asymmetry is computed for all blocks. Since the step size is smaller than the block size, the overlap exists and more values of asymmetry are present for most pixels. To obtain the appropriate asymmetry map, the mean of all values computed for a particular pixel is computed. The computed values of asymmetry create the asymmetry map, which expresses the probability of tumor presence in a particular location. The higher the asymmetry is, the higher is the probability of the tumor presence in a given location.

2.3. Multi-resolution Map

The whole cycle of symmetry checking is repeated four times but with different size of block. Height and width of the block are iteratively reduced to the half of the previous value. So the size of the block is 1/1, 1/4, 1/16, and 1/64 of the initial size, respectively. The purpose of smaller areas is the more precise detection of asymmetry. This approach corresponds to the multi resolution image analysis described in [9]. A block size of 1/256 of the initial size was tested as well, but the results were not improved and the maximum of asymmetry coefficient for this block size was equal to 1 for every image in database.

The output of each cycle is a probabilistic map of anomalies. The product of values corresponding to a particular pixel is computed. The output is the new multi resolution probabilistic map. The example of multi-resolution probabilistic maps are shown in Fig. 1.

2.4. Glioma Extraction

The pathological area extraction is based on the method described in [10], but multi-contrast images, namely T2 and FLAIR, are now involved in this task. In T2-weighted images, glioma and potential edema produce much stronger signal that the white matter, in which they are mostly located. For this reason, the thresholding is employed here. Since the intensities in image can differ from case to case depending on the data acquisition, it has to be computed from the particular image. Moreover, only pixels in the most asymmetric parts have to be involved in the threshold computation. Otherwise, the threshold would be computed incorrectly in case of small tumors. For this purpose, the asymmetry mask is computed. This mask includes the regions, where the asymmetry reached at least 10% of the maximum asymmetry for particular image. Since the result is both-sided mask, healthy and pathological areas are included.

The threshold is determined automatically by Otsu's algorithm [11], but any other automatic method can be used.

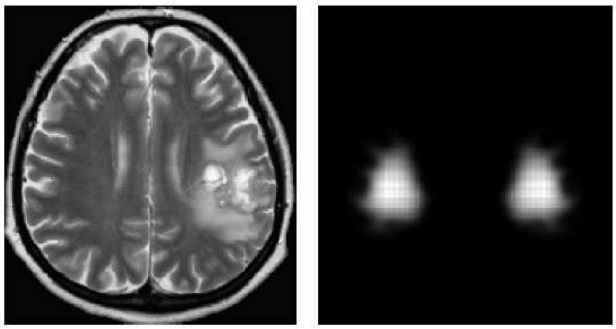

(a) (b)

Figure 1: Asymmetry probabilistic maps for block side length equal to 1/4, 1/8, 1/16, and 1/32 of shorter side of cut image are shown in (a), (b), (c) and (d), respectively. In (e) and (f), input image and total probabilistic map are shown, respectively.

Even though, the threshold is determined only from the image points in the most asymmetric parts, the thresholding process is applied to the whole image. Since some incorrect areas could be extracted, only the regions that have the intersection with the asymmetry mask are labeled as pathological. Regions with the size smaller than 10% of the largest segment are eliminated as well.

Since CSF appears hyper-intense in T2-weighted images as well, the FLAIR volume is employed. In FLAIR the CSF produces much weaker signal than the white matter and the tumor or edema itself. Hence, the areas with the lower intensity than the median intensity (which is most likely the intensity of the white matter) in FLAIR image are eliminated.

3. EXPERIMENTS AND RESULTS

3.1. Datasets

The testing dataset was obtained from the MICCAI 2012 Challenge on Multimodal Brain Tumor Segmentation organized by B. Menze, A. Jakab, S. Bauer, M. Reyes, M. Prastawa, and K. Van Leemput. The challenge database contains fully anonymized images from the following institutions: ETH Zurich, University of Bern, University of Debrecen, and University of Utah.

For each patient, T1, T2, FLAIR, and post-gadolinium T1 MR volumes are available. All volumes are linearly co-registered to the T1 contrast image, skull stripped, and interpolated to 1 mm isotropic resolution.

The data used in algorithm evaluation contains real volumes of 15 high-grade and 7 low-grade glioma subjects. From each case, several slices with pathological area in axial and coronal plane were taken. In total, the extraction algorithm was tested on 357 images with resolution 256×256 pixels in axial plane and on 443 images with resolution 256×181 in coronal plane. Since the proposed method is fully automatic and independent of image intensities, each image of the database can be considered as unique and independent of others. All the simulated images are in BrainWeb space [12]. The information about the simulation method can be found in [13].

3.2. Evaluation Criteria

For the evaluation of region segmentation, Dice Coefficient and Accuracy were used. The Dice Coefficient (DC) (DICE), in some works called Similarity Index, is computed according to the equation

$$\mathrm{DC} = \frac{2\,|A \bigcap B|}{|A| + |B|}, \tag{3}$$

where A and B denotes the ground truth and the result masks of the segmentation, respectively. This criterion compares the intersection of two sets with their union. The range of values of DC is $\langle 0; 1\rangle$, where the value 1 expresses the perfect segmentation. According to [14], the DC $> 0,7$ indicates an excellent similarity.

Another measure widely employed for segmentation evaluation is Accuracy (A), used e.g., in [1] and defined by the equation:

$$A = \frac{TP + TN}{TP + FP + TN + FN}, \tag{4}$$

where TP, FP, FN and TN stand for "True Positive", "False Positive", "False Negative", and "True Negative", respectively. Both measures are in the same range as DC and the higher value indicates the better performance as well.

3.3. Results

This method was tested on 357 axial and 443 coronal images. The summary of the extraction process results is in Table 1. The results are separated according to the tumor type and the slice plane. Slightly better results were achieved for high grade gliomas (HG) than for low grade gliomas (LG).

Table 1: Segmentation evaluation by dice coefficient and accuracy for both planes.

	Axial		Coronal	
	DC	Accuracy	DC	Accuracy
HG	0.86 ± 0.09	0.97 ± 0.03	0.86 ± 0.12	0.96 ± 0.06
LG	0.85 ± 0.12	0.96 ± 0.05	0.79 ± 0.22	0.92 ± 0.12
Overal	0.85 ± 0.11	0.96 ± 0.04	0.82 ± 0.18	0.94 ± 0.10

The worst results were achieved for LG in coronal planes, while in other cases the results are comparable and achieved the value 0.86 for DC and 0.96 for Accuracy. The several results for both planes, both types of glioma and several intervals of resulting DC are shown in Fig. 2.

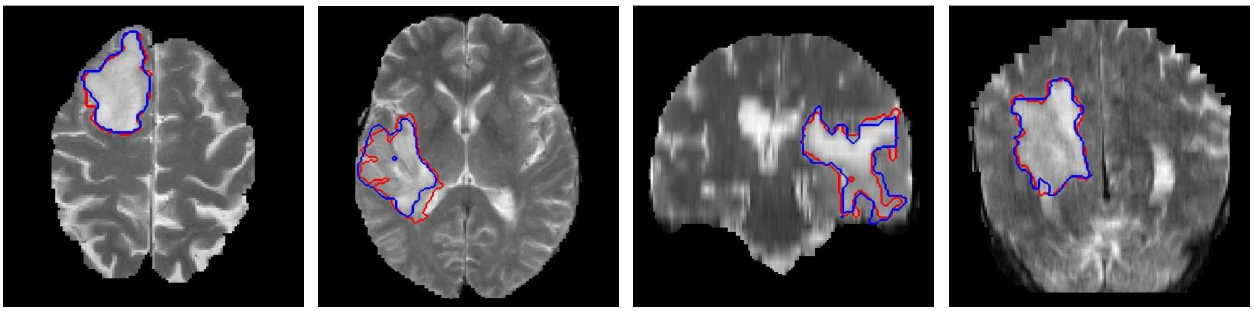

(a) (b) (c) (d)

Figure 2: (a) The average and (b) above-average results for axial slice of low grade glioma and (c) the average and (d) above-average results for coronal slice of high grade glioma. Red: segmentation, Blue: ground truth.

4. CONCLUSION

The aim of this work was an extraction of glioma and edema from 2D MRI images. In axial and coronal plane, the DC coefficient reached value 0.85 ± 0.11 and 0.82 ± 0.18, respectively. Considering the statement that the DC > 0.7 indicates an excellent similarity, the achieved result can be evaluated as very good. Moreover the algorithm considers only information from 2D image and it is fully automated. It is expected that the performance will be improved in future using the neighbor slices information. The accuracy reached values 0.96 ± 0.04 and 0.94 ± 0.10 for axial and coronal plane, respectively. This indicates that in average 95% of pixels were correctly labeled either as pathological or as healthy tissue.

The attention in the future work will also be paid on the relations between neighbor slices and after that, the work will continue with extending the proposed algorithm to 3D. The future work will also consist of implementing the automatic symmetry axis detection, based on literature referred in Section 2, and the separation of the tumor and the edema.

ACKNOWLEDGMENT

The described research is funded by projects SIX CZ.1.05/2.1.00/03.0072, project GACR 102/12/11-04, and project COST CZ LD14091.

REFERENCES

1. Mikulka, J. and E. Gescheidtova, "An improved segmentation of brain tumor, edema and necrosis," *PIERS Proceedings*, 25–28, Taipei, March 25–28, 2013.

2. Wu, Y., W. Yang, J. Jiang, S. Li, Q. Feng, and W. Chen, "Semi-automatic segmentation of brain tumors using population and individual information," *Journal of Digital Imaging*, Vol. 26, No. 4, 786–796, 2013, [Online] Available: http://dx.doi.org/10.1007/s10278-012-9568-1.
3. Pedoia, V., E. Binaghi, S. Balbi, A. De Benedictis, E. Monti, and R. Minotto, "Glial brain tumor detection by using symmetry analysis," *Proc. SPIE*, Vol. 8314, 831445–831445-8, 2012, [Online] Available: http://dx.doi.org/10.1117/12.910172.
4. Zhang, N., S. Ruan, S. Lebonvallet, Q. Liao, and Y. Zhu, "Kernel feature selection to fuse multi-spectral fMRIg images for brain tumor segmentation," *Computer Vision and Image Understanding*, Vol. 115, No. 2, 256–269, 2011, [Online] Available: http://www.sciencedirect.com/science/article/pii/S1077314210002018.
5. Uher, V., R. Burget, J. Masek, and M. Dutta, "3d brain tissue selection and segmentation from mri," *36th International Conference on Telecommunications and Signal Processing (TSP)*, 839–842, 2013.
6. Arce-Santana, E. R. and A. Alba, "Image registration using markov random coefficient and geometric transformation fields," *Pattern Recognition*, Vol. 42, No. 8, 1660–1671, 2009, [Online] Available: http://www.sciencedirect.com/science/article/pii/S0031320308005104.
7. Karuppanagounder, S. and K. Thiruvenkadam, "A novel technique for finding the boundary between the cerebral hemispheres from MR axial head scans," *IICAI*, B. Prasad, P. Lingras, and A. Ram, Eds., 1486–1502, 2009.
8. Bhattacharyya, A., "On a measure of divergence between two statistical populations defined by their probability distribution," *Bulletin of the Calcutta Mathematical Society*, Vol. 35, 99–110, 1943.
9. Kropatsch, W. G., Y. Haxhimusa, and A. Ion, "Multiresolution image segmentations in graph pyramids," *Applied Graph Theory in Computer Vision and Pattern Recognition Studies in Computational Intelligence*, Vol. 52, 3–41, 2007.
10. Dvorak, P., K. Bartusek, and W. G. Kropatsch, "Automated segmentation of brain tumor edema in FLAIR MRI using symmetry and thresholding," *PIERS Proceedings*, 936–939, August 12–15, Stockholm, 2013.
11. Otsu, N., "A threshold selection method from gray-level histograms," *IEEE Transactions on Systems, Man and Cybernetics*, Vol. 9, No. 1, 62–66, 1979, [Online] Available: http://dx.doi.org/10.1109/TSMC.1979.4310076.
12. Prastawa, M., E. Bullitt, and G. Gerig, "Simulation of brain tumors in MR images for evaluation of segmentation efficacy," *Medical Image Analysis*, Vol. 13, No. 2, 297–311, 2009, [Online] Available: http://www.sciencedirect.com/science/article/pii/S1361841508001357.
13. Cocosco, C. A., V. Kollokian, R. K.-S. Kwan, G. B. Pike, and A. C. Evans, "Brainweb: Online interface to a 3d mri simulated brain database," *NeuroImage*, Vol. 5, 425, 1997.
14. Zijdenbos, A. and B. Dawant, "Brain segmentation and white matter lesion detection in mr images," *Critical Reviews in Biomedical Engineering*, Vol. 22, 401–465, 1994.